Sedimentation Analysis of Novel DNA Structures Formed by Homo-Oligonucleotides

Danny M. Hatters,* Leanne Wilson,* Benjamin W. Atcliffe,* Terrence D. Mulhern,* Nancy Guzzo-Pernell,† and Geoffrey J. Howlett*

*Department of Biochemistry and Molecular Biology and †Howard Florey Institute of Experimental Physiology and Medicine, The University of Melbourne, Parkville, Victoria 3010, Australia

ABSTRACT Sedimentation velocity analysis has been used to examine the base-specific structural conformations and unusual hydrogen bonding patterns of model oligonucleotides. Homo-oligonucleotides composed of 8–28 residues of dA, dT, or dC nucleotides in 100 mM sodium phosphate, pH 7.4, at 20°C behave as extended monomers. Comparison of experimentally determined sedimentation coefficients with theoretical values calculated for assumed helical structures show that dT and dC oligonucleotides are more compact than dA oligonucleotides. For dA oligonucleotides, the average width (1.7 nm), assuming a cylindrical model, is smaller than for control duplex DNA whereas the average rise per base (0.34 nm) is similar to that of B-DNA. For dC and dT oligonucleotides, there is an increase in the average widths (1.8 nm and 2.1 nm, respectively) whereas the average rise per base is smaller (0.28 nm and 0.23 nm, respectively). A significant shape change is observed for oligo dC_{28} at lower temperatures (10°C), corresponding to a fourfold decrease in axial ratio. Optical density, circular dichroism, and differential scanning calorimetry data confirm this shape change, attributable from nuclear magnetic resonance analysis to i-motif formation. Sedimentation equilibrium studies of oligo dG_8 and dG_{16} reveal extensive self-association and the formation of G-quadruplexes. Continuous distribution analysis of sedimentation velocity data for oligo dG_{16} identifies the presence of discrete dimers, tetramers, and dodecamers. These studies distinguish the conformational and colligative properties of the individual bases in DNA and their inherent capacity to promote specific folding pathways.

INTRODUCTION

Certain DNA sequences adopt unusual hydrogen bonding patterns and structural conformations both in vitro and within genomes. An example is triple helical DNA, comprised of two strands coupled by Watson-Crick base pairing and a third strand bonded in the major groove through Hoogsteen base pairing (Arnott et al., 1976). Such complexes have potential as new therapeutic agents for the disruption of specific genes (Guzzo-Pernell et al., 1997). Analysis of unusual DNA structures accelerated with the discovery that the telomeric ends of eukaryotic chromosomes are composed of simple repeating sequences containing short tracts of guanine residues alternating with short tracts of A/T-rich sequences (Blackburn, 1984). Nuclear magnetic resonance (NMR) and x-ray crystallographic studies show both parallel and anti-parallel G-quadruplex structures stabilized by Hoogsteen hydrogen bonding (Kang et al., 1992; Laughlan et al., 1994). Guanine-rich regions with novel DNA folds have now been associated with centromeres (Ferrer et al., 1995), recombination (Venczel and Sen, 1996), hyper-variable regions in mini-satellite DNA (Weitzmann et al., 1998), fragile X syndrome (Kettani et al., 1995), and promoter regions upstream of the human insulin gene (Catasti et al., 1996) and chicken β-globin genes (Howell et al., 1996). At low pH, cytosine-rich strands also form four-stranded structures but with a different architecture. These tetraplexes, or i-motif, are formed by base pairing of hemi-protonated C strands ($C.C^+$) intercalated with another pair of C-strands, analogous to two off-set perpendicular ladders (Gehring et al., 1993). Formation of i-motif in C-rich telomeric and centromeric sequences may facilitate the structural role of the G-rich regions contained in the complementary strand (Ahmed and Henderson, 1992). For the fragile X DNA triplet repeat the propensity of hairpin formation appears to be more pronounced for the C-rich strand than for the G-rich strand (Chen et al., 1995)

In vitro studies on novel DNA structures have mainly involved synthetic oligonucleotides based on naturally occurring sequences. X-ray crystallographic studies of *Oxytricha* telomeric DNA show G quadruplexes with loops containing T residues at either ends (Kang et al., 1992) whereas both T and A residues have been observed in the loops of C-rich four-stranded structures (Leroy et al., 1994). The role of A and T residues as determinants of DNA folds is not clear although T residues may play a specific role in loops by providing single-strand flexibility (Guo et al., 1993).

The inherent capacity of the different bases in DNA to promote specific structures is difficult to delineate using oligonucleotides composed of different bases. Homo-oligonucleotides, containing linked residues of identical nucleotides, permit a direct comparison of the properties of the individual bases. X-ray diffraction patterns of polyriboguanylic acid indicate self-association consistent with a four-

Received for publication 12 January 2001 and in final form 30 March 2001.

Address reprint requests to Dr. Geoffrey Howlett, University of Melbourne, Parkville, Russel Grimwade School of Biochemistry and Molecular Biology, Parkville, Victoria 3010, Australia. Tel.: 61-3-8344-7632; Fax: 61-3-9347-7730; E-mail: ghowlett@unimelb.edu.au.

0006-3495/01/07/371/11 $2.00

stranded model (Zimmerman et al., 1975) whereas x-ray diffraction studies of polycytidylic acid, at low pH, have been interpreted as parallel two-stranded helical structures (Langridge and Rich, 1963). Temperature-dependent circular dichroism of deoxyadenylates indicates nucleotide stacking of single-stranded oligomers into a geometry resembling that of B-DNA (Olsthoorn et al., 1981).

Our recent development of sedimentation velocity methods to determine the rate of sedimentation of small peptides (Schuck et al., 1998) suggested a new approach for the analysis of the conformational state and extent of self-association of small oligonucleotides. In this study we apply these and other techniques to define the inherent capacity of a series of dA, dT, dC, and dG oligonucleotides to fold and interact to form specific structures in solution.

MATERIALS AND METHODS

Sets of dA, dC, and dT oligonucleotides containing 8, 12, 16, 20, 24, and 28 residues and dG oligonucleotides containing 8 and 16 residues were used in this study. Oligo dA nucleotides were purchased from Pacific Oligos (Toowoomba, Australia). Other oligonucleotides were synthesized using standard β-cyanoethyl nucleoside phosphoramidites and automated 1 μmol DNA synthesis. The crude oligonucleotides were fractionated by denaturing polyacrylamide gel electrophoresis and the relevant bands excised and eluted in 0.1 mM EDTA for 48 h. The eluted product was purified by reversed-phase HPLC using buffer A (0.1 M triethyl ammonium acetate, pH 7.0) and buffer B (acetonitrile) with a gradient of buffer B from 0–50%. Fractions were collected and lyophilized and the oligonucleotide yield determined spectrophotometrically (Cantor et al., 1970).

Analytical gel electrophoresis

The molecular state of the oligonucleotides was analyzed by nondenaturing gel electrophoresis with 20% polyacrylamide gels using a mini Protean II system (Bio-Rad, Hercules, CA). Oligonucleotide samples in 10 μl (OD_{260} in the range 20–70) were mixed with 4 μl of 30% glycerol and loaded onto the gel. After electrophoresis the DNA was visualized by UV shadowing against a DC-Alufolien Kieselgel 60 F_{254} TLC plate (Merck, Darmstadt, Germany).

Analytical ultracentrifugation

Before sedimentation velocity analysis oligo dA, dT, and dC were further purified by gel filtration chromatography using a Sephadex G-50 column (HR10–30, Pharmacia, Uppsala, Sweden) pre-equilibrated in 100 mM sodium phosphate, pH 7.4. The column was run at a flow rate of 0.5 ml/min and the eluent monitored at 280 nm. For the oligo dG_8 and dG_{16} sedimentation analysis was performed on both the unfractionated samples and on the peaks that eluted from gel filtration performed as described above. Samples, with optical densities at 260 nm in the range 0.15–1.0, were analyzed by analytical ultracentrifugation (XLA analytical ultracentrifuge, Beckman/Coulter, Fullerton, CA) using double sector filled epon centerpieces. The rotor speed was 30,000 rpm and the temperature 20°C unless indicated. Fluorochemical FC-43 oil (20 μl) was used in the sample and reference compartments to allow identification of the bottom of the cell. Radial optical densities were measured at 260 nm using 0.002-cm radial intervals and a continuous scan setting. Samples were temperature equilibrated at 3000 rpm for 1–2 h before the velocity was increased to the final speed indicated.

Computational analysis

Sedimentation equilibrium profiles in the form of optical density versus radial distance were analyzed using the program SEDEQ1B (Minton, 1994) to obtain values for the buoyant molecular mass given by the product $M(1 - v\rho)$ where M is the molecular mass of the solute, v the partial specific volume, and ρ the solution density. Direct fitting of sedimentation velocity data with numerical solutions of the Lamm equation was performed using sequential radial scans taken during the approach to equilibrium and the program SEDFIT as described previously (Schuck et al., 1998). For fitting to a single species, the data were analyzed by floating both the sedimentation coefficient and molecular mass. For all samples, the best-fit values obtained for the sedimentation coefficient and molecular mass were similar regardless of whether the baseline was fixed or floated with the best-fit value for baseline close to zero. Error bars were calculated by F-statistics with the confidence interval set at $p = 0.68$. Data for the dG oligonucleotides were also fitted to a continual mass distribution (Schuck, 2000) with the confidence interval set at $p = 0.68$ and the baseline absorbance set to zero.

Hypothetical A, B, and Z single-stranded oligonucleotide structures were generated using the software package HyperChem (Hypercube, Ontario, Canada) and used to compute sedimentation coefficients using the program HYDROPRO (Garcia de la Torre et al., 2000). The atomic size parameter required for the bead modeling was 3.2 Å, an average value derived from the analysis of 13 well characterized proteins (Garcia de la Torre et al., 2000). Buffer densities, viscosities, and sedimentation coefficients for prolate ellipsoids or cylinders were calculated using the program SEDNTERP (Laue et al., 1992). A value of 0.9 g/g was assumed for the hydration of oligonucleotides based on the average value obtained from previous studies of isotropic 6–8-base-pair DNA duplexes (Bonifacio et al., 1997).

Differential scanning calorimetry

A 0.5-ml sample of dC_{28} (29 μM) containing 100 mM sodium phosphate, pH 7.4, in the sample compartment was scanned against 100 mM sodium phosphate, pH 7.4, in the reference compartment in a VP-differential scanning calorimeter (MicroCal, Northampton, MA). The temperature was ramped from 5°C to 45°C at a scan rate of 60°C/h with the post cycle thermostat set at 5°C. Ten scans were collected with a filtering period of 20 s and with feedback mode on passive gain. Scans were also performed from 45°C to 5°C at a scan rate of 45°C/h. Baseline spectra were recorded under the same conditions with buffer versus buffer in the two compartments. Data were analyzed with the software provided by the equipment manufacturer to correct for baseline effects and the differential heat capacities for the folded and unfolded states to obtain the enthalpy of unfolding.

NMR spectroscopy

Samples were prepared in 100 mM sodium phosphate, pH 7.4 or pH 6.0, with the addition of ^2H_2O to 10%. All NMR spectra were recorded on Varian Inova 500- and 600-MHz spectrometers (Varian, Palo Alto, CA). Water suppression was achieved by lower power presaturation during the relaxation delay (1.5 s) and during the mixing time (150 ms) in two-dimensional (2D) nuclear Overhauser effect spectroscopy (NOESY) experiments. The residual water signal was further attenuated by solvent subtraction during data processing. The 2D total correlation spectroscopy (TOCSY) experiments were recorded with a 50-ms spin-lock period. Spectra were centered on the water signal and experiments were recorded with spectral widths of 10.0 ppm or, if the $C.C^+$ imino protons were to be observed, 26.0 ppm. The 1D experiments were acquired over 8192 data points, and 2D experiments were acquired over 2048 or 4096 data points in F2 for 10.0 ppm or 26.0 ppm spectral widths, respectively. In all 2D

experiments 128 complex points were collected (with a minimum of 64 transients recorded per T1 increment), and these data were used to forward linear predict a further 128 complex points. Data were processed using VNMR 6.1B (Varian, Palo Alto, CA) and spectra analyzed using XEASY (Bartels et al., 1995). The 1D spectra were processed after application of a Gaussian window function with 20-Hz line broadening. The 2D TOCSY and NOESY spectra were processed after the application of cosine-squared window functions and 20-Hz line broadening. The 2D double quantum filtered correlation spectroscopy (DQF-COSY) spectra were processed with a Gaussian function in T2 and an unshifted sine bell in T1. Spectra were referenced via the H_2O signal, the temperature dependence of its chemical shift having been calibrated to 2,2-dimethyl-2-sialapentane-5-sulfonic acid (DSS) (0.0 ppm) in a separate sample. Data were recorded at temperatures from −5°C to 60°C. When changing probe temperature, a minimum of 15 min was allowed before shimming, for thermal equilibration of the sample.

Circular dichroism (CD) spectroscopy

CD spectra were recorded in a model 62DS AVIV (Lakewood, NJ) CD spectrometer. The spectra were measured in 1-cm quartz cuvettes and data collected from 330–220 nm at 0.5-nm intervals with 1-s integration time. The samples were in 100 mM sodium phosphate, pH 7.4. The bandwidth was set at 1.5 nm and temperature controlled by a Peltier water bath. The mean nucleotide ellipticity, $[\theta]$, was calculated from the equation $[\theta] = \theta/(cnl)$ where l is path length in cm, θ is observed ellipticity in millidegrees, c is the molar concentration of oligonucleotide, and n is number of nucleotide residues. Spectra were corrected for baseline using the spectrum for buffer alone.

Hyperchromicity measurements

The absorbances of the oligonucleotides dissolved in 100 mM sodium phosphate, pH 7.4, were measured in a Cary-5 spectrophotometer (Varian, Australia) in 1-cm quartz cuvettes at 240 nm. The temperature was ramped at 0.5°C min^{-1} from 10°C to 70°C with the temperature controlled by a Peltier waterbath. Scans were also recorded from 70°C to 5°C at the same scan rate.

RESULTS

Buoyant molecular mass analysis of dA, dC, and dT oligonucleotides

An essential step in the interpretation of sedimentation data for oligonucleotides is the determination of the buoyant molecular masses, $M(1 - \nu\rho)$, of the sedimenting species. Analysis of sedimentation equilibrium distributions for dA, dC, and dT oligonucleotides composed of 8, 12, 16, 20, 24, and 28 bases gave buoyant molecular mass values indicative of single sedimenting species. Assuming an approximate value of 0.55 ml/g for the partial specific volume of DNA (Durchschlag, 1986), the derived molecular mass values indicated that the oligonucleotides were monomeric. A more extensive analysis of the data involved global analysis of sequential scans taken during the approach to equilibrium (Schuck et al., 1998). Excellent fits assuming a single sedimenting species were obtained with the residuals close to randomly distributed with root mean square deviation (rmsd) < 0.011. Fig. 1 shows that the buoyant molecular masses are a linear function of the compositional molecular masses, implying a constant buoyant density term over this range. The slope of the line drawn through the data yields $1 - \nu\rho$ values for the different sets of oligonucleotides and hence ν, from the known solution density (Table 1). For comparison, a double-stranded oligonucleotide duplex, $dA_{16}.dT_{16}$, was also examined, yielding a buoyant molecular mass of 4082 (rmsd = 0.003), corresponding to a calculated apparent partial specific volume of 0.58 ml/g (Table 1). This value is intermediate between the values obtained for the constituent oligo dA and dT strands.

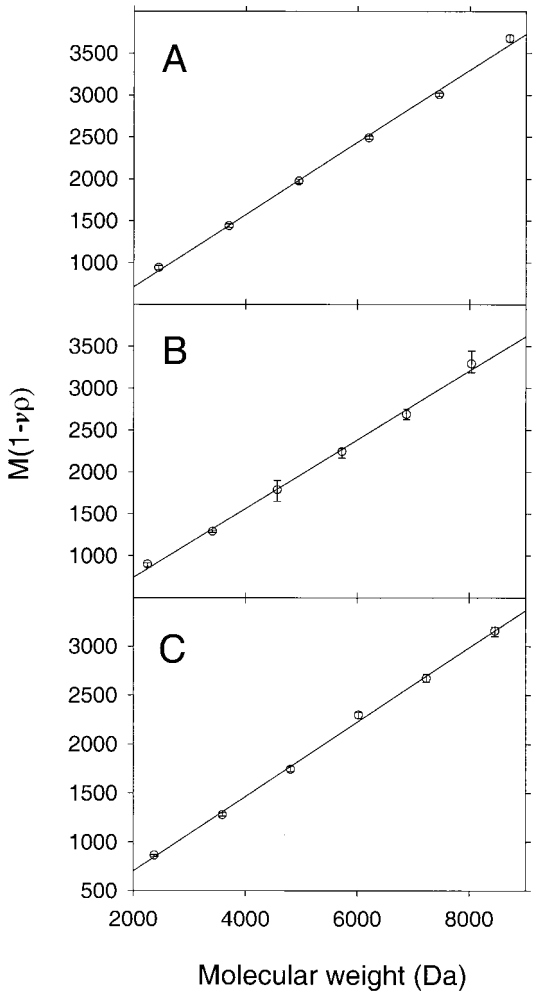

FIGURE 1 Buoyant molecular mass values (M[1 − $\nu\rho$]) for oligonucleotides. Values for dA, dC, and dT oligonucleotides (*A*, *B*, and *C*, respectively) are plotted as a function of the compositional molecular mass. Error bars were calculated using F-statistics ($p = 0.68$) as described in Materials and Methods.

Sedimentation velocity analysis

In addition to providing buoyant molecular mass values, global analysis of sedimentation velocity data also provides estimates of the sedimentation coefficients. These latter

TABLE 1 Apparent partial specific volume of deoxyoligonucleotides from sedimentation analysis

Oligonucleotide	v' (ml/g)
dA*	0.56
dC*	0.58
dT*	0.61
dG†	0.54
dAT‡	0.58

*Values for the apparent partial specific volumes (v') of dA, dC, and dT oligonucleotides were obtained by regression analysis of the lines drawn through the data in Fig. 1.

†The apparent partial specific volume of dG_{16} was deduced from sedimentation equilibrium analysis of peak 2 (Fig. 9) using a value of 10,258 for the molecular mass of the dG_{16} dimer.

‡A duplex of dA_{16} and dT_{16} was purified by gel filtration and the apparent partial specific volume calculated from sedimentation analysis assuming a value of 9754 for the molecular mass of the duplex.

values depend on the shape of the sedimenting solutes and show a nonlinear increase as a function of the number of constituent bases (Fig. 2). Theoretical sedimentation coefficients calculated for these oligonucleotides, assuming structures corresponding to single helical strands of either A, B, or Z double-stranded DNA, are included in Fig. 2. These computed values emphasize the dependence of sedimentation rates on oligonucleotide conformation and permit interpretation of the experimental values.

The experimentally determined sedimentation coefficients of the dA oligonucleotides are generally lower than the values calculated for any of the helical configurations. Although these deviations may indicate a limitation of the theoretical calculations there are other valid interpretations. NMR studies indicate that the majority of oligo dA (70%) stacks in a B-DNA-like structure with the remainder in an undefined configuration (Olsthoorn et al., 1981). Transitions between such structures could account for the deviations shown in Fig. 2 *A*. Alternatively, single-stranded oligo dA nucleotides may adopt a slightly more extended configuration than that observed in typical double-stranded B-DNA.

In contrast to the observations with the dA oligonucleotides, the experimentally determined sedimentation coefficients for dC and dT oligonucleotides generally lie above the values calculated for hypothetical single-stranded, B-DNA structures (Fig. 2). These higher values suggest reduced frictional coefficients, consistent with more compact structures. Direct estimates of the frictional coefficients and axial ratios for the oligonucleotides were obtained by combining the results from Figs. 1 and 2. The results in Fig. 3 show that the frictional coefficients and axial ratios for oligo dA, dC, and dT 8-mers are close to unity, indicating that these small oligomers are essentially isotropic. The axial ratios for the larger oligonucleotides increase systematically with the greatest increase observed for the dA oligomers. This shows that dA oligonucleotides are more rod-like and

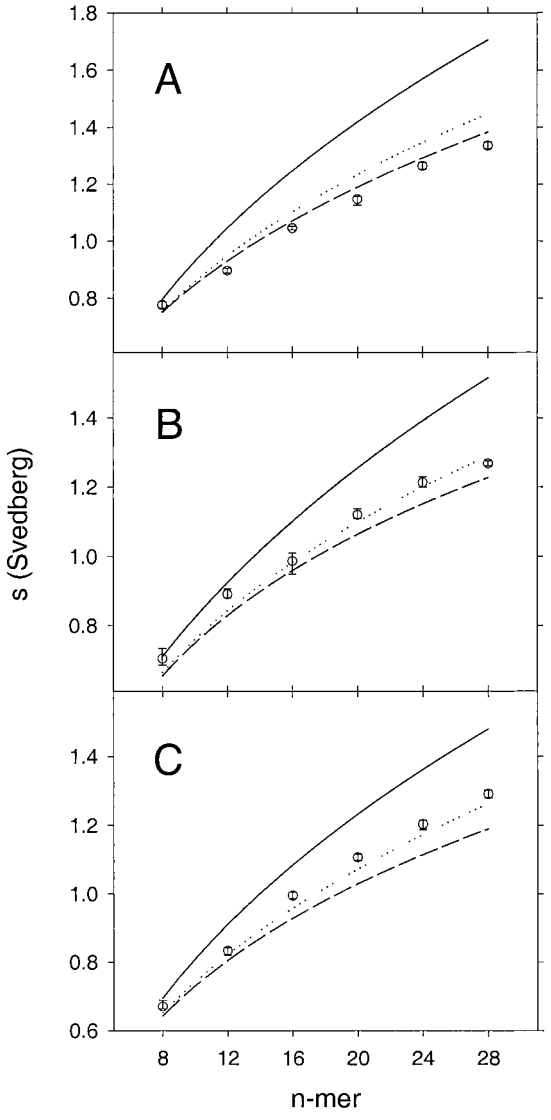

FIGURE 2 Sedimentation coefficients of the dA, dC, and dT oligonucleotides as a function of oligonucleotide length in bases (*A*, *B*, and *C*, respectively); ○, measured sedimentation coefficients. Error bars were calculated using F-statistics ($p = 0.68$). Hypothetical sedimentation coefficients for single-stranded oligonucleotides in A-form DNA (——), B-form DNA (· · ·), and Z-form DNA (— — —) are shown.

less compact than the corresponding dC and dT structures, in accord with the conclusions drawn from Fig. 2.

Further insight into the shape of the larger oligonucleotides is provided from calculations based on an assumed cylindrical geometry (Laue et al., 1992). We initially analyzed the data for the control $dA_{16}.dT_{16}$ duplex. Computed values, based on the sedimentation coefficient, 1.603 S (+0.025, −0.017), molecular mass, and apparent partial specific volume (Table 1) indicate a frictional ratio (f/f_0) of 1.64 corresponding to a cylindrical width of 2.2 nm and a rise per base pair of 0.39 nm. These latter values are in reasonable agreement with values of 2.3 nm and 0.34 nm,

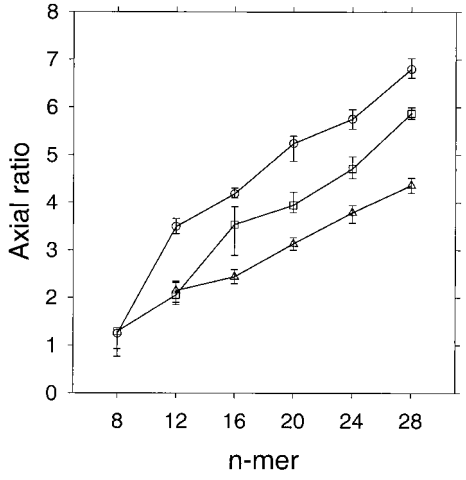

FIGURE 3 Axial ratios of dA, dC, and dT oligonucleotides based on an ellipsoid model. Axial ratios for dA (○), dC (△), and dT (□) oligonucleotides are plotted as a function of the nucleotide length in bases. Error bars were calculated from the minimum and maximum sedimentation coefficients (Fig. 2).

TABLE 2 The cylindrical dimensions of dA, dC, and dT oligonucleotides

	dA		dC		dT	
n-mer	Width	Length/base	Width	Length/base	Width	Length/base
20	1.68	0.34	1.86	0.26	2.11	0.22
24	1.71	0.33	1.82	0.27	2.06	0.23
28	1.68	0.34	1.75	0.29	2.04	0.23

Cylindrical dimensions of width and length per base (in nm) were calculated from the buoyant molecular masses and sedimentation coefficients in Fig. 1 and 2. Analysis of smaller oligonucleotides revealed aspect ratios (p = length/width) of less than 2, which is outside the limits for this analysis ($2 < p < 20$).

respectively, determined for B-DNA (Wing et al., 1980). For dA oligonucleotides comprised of 20, 24, or 28 nucleotides, the results for a cylindrical model (Table 2) show an average width of 1.7 nm and rise per base of 0.34 nm. This average width is smaller than that obtained for the control duplex DNA as might be expected for a single-stranded compared with a double-stranded helix whereas the average rise per base is the same as that of B-DNA. The average rise per base is smaller for the dC and dT oligonucleotides (0.28 nm and 0.23 nm, respectively) compared with oligo dA, whereas there is an increase in the average widths (1.8 nm and 2.1 nm, respectively). These results therefore support the conclusion that dC and dT oligonucleotides are more compact than the corresponding dA oligonucleotides.

Conformational analysis of oligo dA, dC, and dT

We next examined the secondary structure of the oligonucleotides by CD spectroscopy. CD spectra for dA oligonucleotides containing 8, 12, 16, 20, 24, and 28 bases, expressed per residue, all superimposed with representative data presented in Fig. 4 for oligo dA_8 and dA_{28}. The overlap indicates a similar secondary structure for all of the dA oligomers, consistent with a simple repeating helical structure. In contrast, the CD spectrum for the set of dC oligonucleotides varied systematically, with the extremes represented by the spectra for oligo dC_8 and dC_{28} in Fig. 4. The systematic change in the wavelength of the ellipticity maximum from 280 nm to 282.5 nm for oligo dC_8 through to oligo dC_{28} nucleotides and the increase in the ellipticity signal demonstrate length-dependent differences in the secondary structure of dC oligonucleotides. CD spectra for the set of dT oligonucleotides showed no change in the wavelength of the ellipticity maximum and minimum and a small change in the magnitude of the ellipticity signal of dT_8 compared with dT_{28} (Fig. 4). The temperature dependence of the CD spectrum for the oligonucleotide 28-mers was also examined. For oligo dA_{28} and oligo dT_{28} the spectra obtained at 25°C and 70°C were not significantly different. However, for oligo dC_{28} there was a decrease of ~40% in the ellipticity at 280 nm and 70°C compared with 25°C,

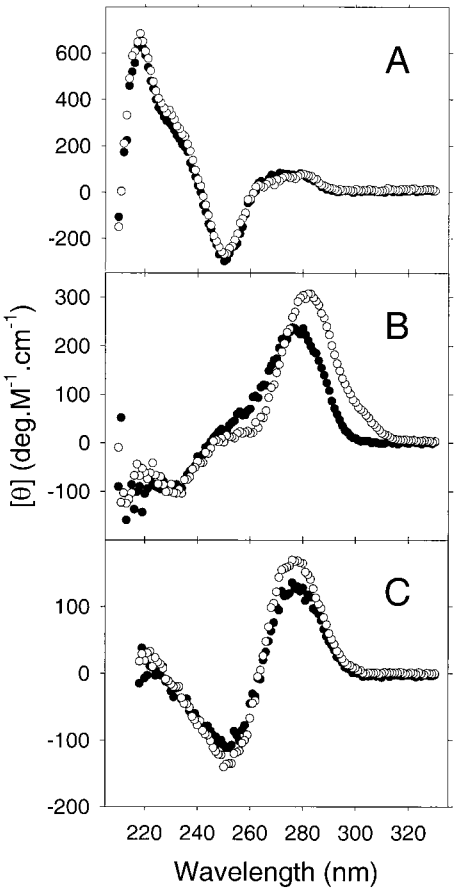

FIGURE 4 Circular dichroism spectra of dA, dC, and dT oligonucleotides at 20°C (*A*, *B*, and *C*, respectively); ●, 8-mers; ○, 28-mers.

which taken together with the observed change in the CD spectra as a function of oligonucleotide length, suggests significant length-dependent conformational flexibility.

Temperature-dependent folding of oligo dC

Several techniques were used to further explore the conformational states of the dC oligonucleotides. Fig. 5 *A* shows large changes in the optical densities of oligo dC_{24} and dC_{28} solutions as a function of temperature. These larger hyperchromic changes over the temperature range 10–35°C indicate heat-induced, cooperative unfolding. At a constant scan rate (0.5°C min^{-1}), the midpoints for unfolding of dC_{24} and dC_{28} were 14°C and 17°C, respectively. Cooperative changes in optical densities were not observed in experiments with oligo dC_{12}, dC_{16} (not shown), and dC_{20} (Fig. 5 *A*) over the same range of temperatures. Absorbance profiles for oligo dA_{28} and oligo dT_{28} indicated small, gradual rises of ~4% and 1% over the temperature range 10–35°C. These changes are similar to previous studies (Cassani and Bollum, 1969).

Differential scanning microcalorimetry was also used to investigate the heat-induced cooperative transition associated with oligo dC_{28}. The data in Fig. 5 *B* fit well to a two-state endothermic transition with a midpoint of melting of 20.7°C and an apparent enthalpy of unfolding of 260 kJ/mol or 9.3 kJ/residue. This latter value may be compared to values reported for thermal dissociation transitions for DNA/DNA duplexes, which range from 3.6 to 11.8 kJ/residue (Chakrabarti and Schwartz, 1999). Although sequential up-scans and down-scans were highly reproducible and indicated a reversible transition, differences between the two sets of scans showed hysteresis, implying a relatively slow folding and unfolding process (Leroy et al., 1994).

Shape changes accompanying the unfolding of oligo dC_{28} were examined by sedimentation velocity experiments

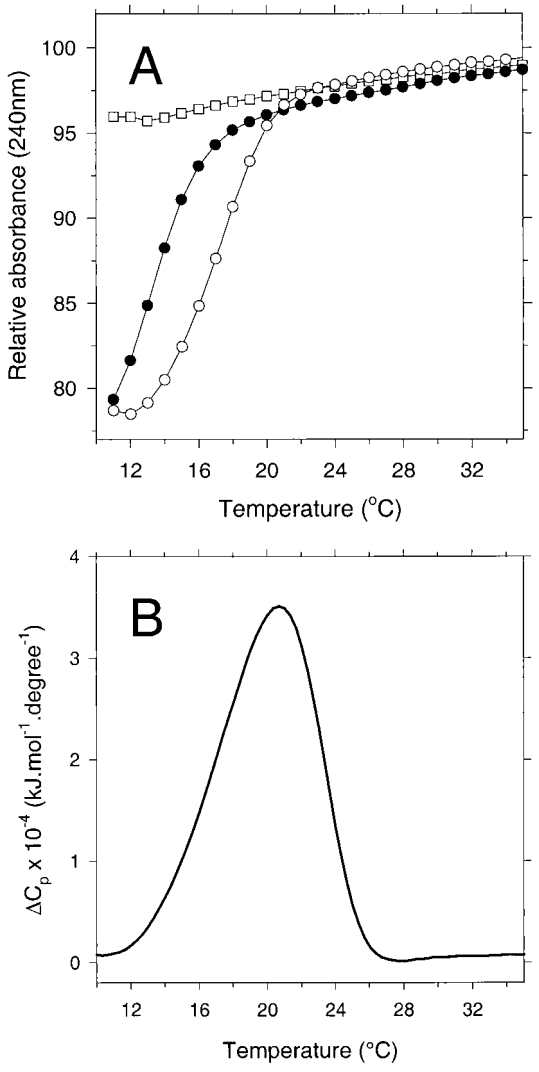

FIGURE 5 (*A*) Temperature dependence of relative optical densities of dC_{20}, dC_{24}, and dC_{28} oligonucleotides. The relative optical densities are expressed as a percentage of the absorbances at 70°C for oligo dC_{20} (□), dC_{24} (●), and dC_{28} (○). (*B*) Differential scanning calorimetry of oligo dC_{28}. The data have been corrected for ΔC_p contributions of the folded and unfolded states and for buffer baseline.

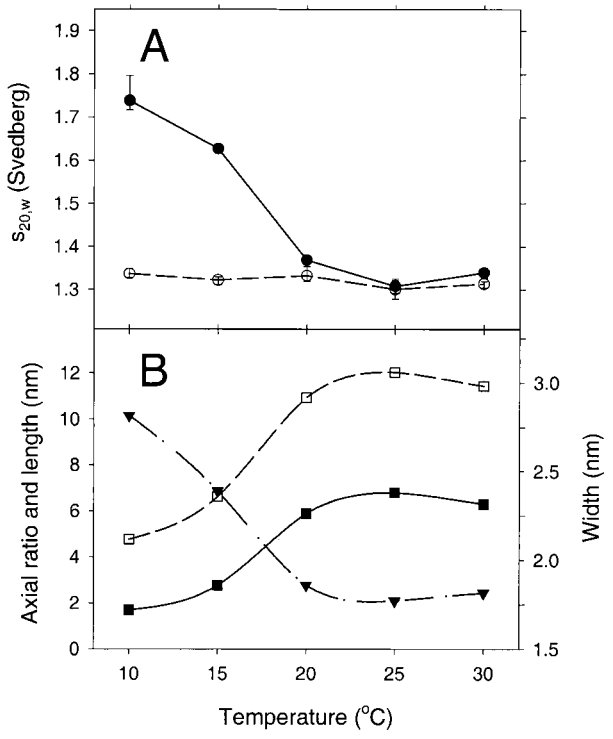

FIGURE 6 (*A*) Sedimentation coefficients ($s_{20,w}$) of oligo dC_{28} (●) and dT_{28} (○) as a function of temperature. Error bars were calculated by F-statistics ($p = 0.68$). (*B*) Calculated values for dC_{28} assuming an ellipsoid model (axial ratio, width, and length). The axial ratio (■), width (▲), and length (□) parameters were calculated for the data for dC_{28} in *A*.

across the transition range of temperatures. Temperature-corrected, best-fit values for the sedimentation coefficients for oligo dC_{28} show a large decrease from 1.75 S at 10°C to 1.35 S at 30°C, in contrast to results obtained for oligo dT_{28} where no significant changes are observed (Fig. 6 *A*). Over this same temperature range there was essentially no change in the molecular mass of oligo dC_{28} with values of 2880 (+90, −70), 3040 (+60, −80), 3240 (+60, −80), 2960 (+40, −180), and 3010 (+90, −70) obtained at temperatures of 10°C, 15°C, 20°C, 25°C, and 30°C, respectively. This suggests that the temperature-induced changes in the average sedimentation coefficients are due to an alteration in shape rather than aggregation state. Analysis according to an ellipsoid model indicates the average axial ratios varied from 1.7 at 10°C to 6.8 at 25°C with corresponding changes in the average length and width parameters consistent with either a two-state or sequential transition to a longer, thinner shape at 30°C (Fig. 6 *B*).

NMR analysis

The temperature-dependent transition observed for oligo dC_{28} suggested the presence, at low temperatures, of a folded monomeric structure. C-rich oligonucleotides, such as the $d[CCCTAA]_3CCC$ (Leroy et al., 1994) and $d(5mCCT_3CCT_3ACCT_3CC)$ (Han et al., 1998), fold to form an i-motif, which is a four-stranded structure in which two parallel-stranded duplexes associate via intercalation of hemiprotonated $C.C^+$ base pairs with the A and T nucleosides in the inter-strand loops. The i-motif can also form by the tetramerization of shorter C-rich oligonucleotides such as $d(TC_5)$ and $d(T_2C_4T_2)$ (Leroy et al., 1993). Therefore, the possibility of intramolecular i-motif formation by dC_{28} was examined by NMR spectroscopy.

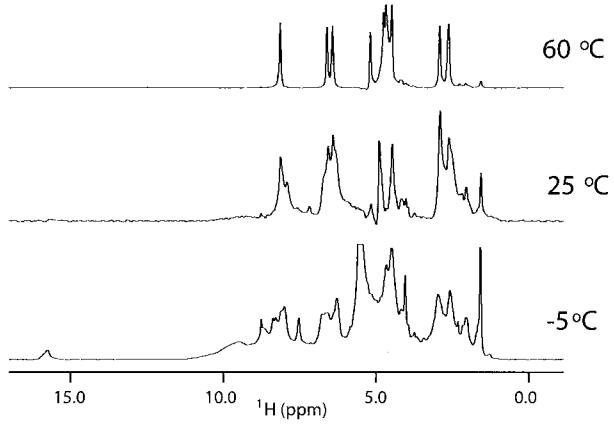

FIGURE 7 Temperature dependence of ^1H NMR spectra of oligo dC_{28}. Spectra were recorded from samples in 100 mM sodium phosphate, pH 6.0, and the one-dimensional ^1H NMR spectrum of oligo dC_{28} is shown at 60°C, 25°C, and −5°C.

The ^1H NMR spectrum of dC_{28} at temperatures well above its melting point was very similar to that measured for 2-deoxycytidine. However, upon cooling, the spectrum became considerably more complex and exhibited line broadening (Fig. 7). The broadness of the lines, complexity of the spectrum, and the lack of chemical shift dispersion prevented us from detailed structural interpretation. However, analysis of 2D DQF-COSY, TOCSY, and NOESY data at 40°C and −5°C and comparison of chemical shift assignment data with that of well characterized i-motif (Han et al., 1998; Nonin and Leroy, 1996) suggested the formation of such a structure by dC_{28}. At high temperatures no signals were present from the exchangeable H4 amine protons; however, upon cooling these resonances were observed at ~8.4 ppm (H4 *trans*) and 9.0–9.5 ppm (H4 *cis*). In addition, a weak resonance at 15.6 ppm was also observed upon cooling. This signal is characteristic of the shared cytidine $N3H^+$ imino proton in the $C.C^+$ pairings of i-motif. By reducing the pH of the dC_{28} sample from 7.4 to 6.0 the intensity of the imino and amine signals increased approximately threefold, whereas the rest of the spectrum remained essentially the same, suggesting that the change in pH did not alter the overall structure of the molecule but reduced the effects of chemical exchange at these sites. The increased intensity of the exchangeable proton signals allowed us to observe NOEs involving these groups, including NOEs between the H4 amine protons and deoxyribose H2′ and H2″ protons (Fig. 8). These NOEs are characteristic

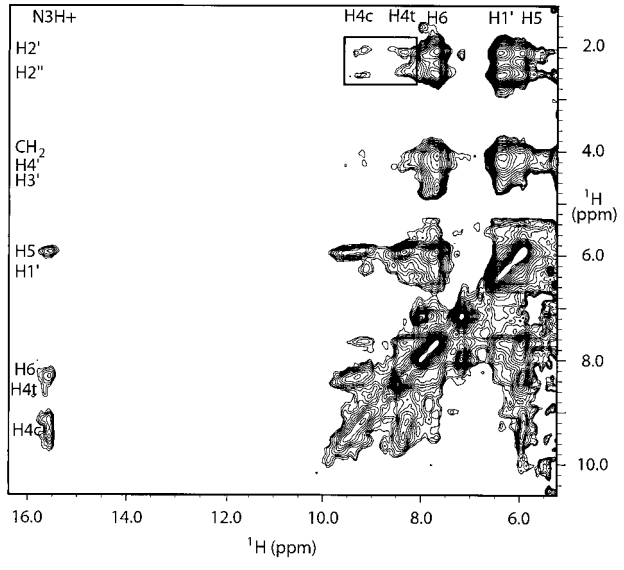

FIGURE 8 A region of the ^1H-^1H NOESY spectrum of oligo dC_{28} at −5°C. The spectrum was recorded from a sample at pH 6.0. The approximate chemical shifts of base and sugar ring hydrogens that are observable in this region are marked along the axes. H4c and H4t refer to the *cis* and *trans* H4 amide hydrogens, respectively. NOEs between the H4 amide group and the H2′ and H2″ hydrogens of the sugar ring, which are characteristic of the i-motif conformation, are boxed.

of the short distances in the i-motif between the amine group in one strand and a sugar ring in the antiparallel strand across the major groove (Leroy et al., 1994). Comparison of the integrated intensity of the nonexchangeable H5 and H1 protons with that of the imino signal at pH 6.0 and −5°C indicated the presence of approximately eight imino protons in the structure, consistent with the pairing of four bases from each strand and loops of three to four nucleotides in length, depending on whether there are any unpaired nucleotides at the 5′ and 3′ ends. The broadening of the dC_{28} NMR spectrum upon cooling is suggestive of conformational exchange between multiple species. Similar broadening has been observed for the i-motif formed by the vertebrate telomere fragment $d[CCCTAA]_3CCCT$ (Phan et al., 2000). In that case the source of the broadening was identified as conformational exchange in the two loops at the bottom of the structure. We could expect similar effects in dC_{28} as well as the possibility that because the loop positions are not dictated by the presence of A or T residues, a number of species, all based around four strands that are four C residues in length but having loops and tails of varying lengths, could exist in exchange with one another. An additional source of line broadening at low temperatures could be the slower rotational correlation times caused by increased solvent viscosity and the formation of a small amounts of higher oligomers in the pH 6.0 sample, as demonstrated by sedimentation equilibrium analysis (results not shown). The later effect is likely to be minimal as similar line broadening was observed in NMR spectra at pH 7.0 where no evidence of self-association was detected by sedimentation equilibrium.

Self-association of oligo dG

In contrast to our results with dA, dC, and dT oligonucleotides, our studies with dG oligonucleotides indicated a propensity to self-associate as indicated by the results in Fig. 9. Gel electrophoresis of oligo dG_8 resolves two major bands whereas for oligo dG_{16} three major bands are readily identifiable (Fig. 9 *A*). The electrophoretic mobility of the faster migrating oligo dG_8 band corresponds to the mobility of dA_{16} and dC_{16} oligomers, suggesting that this species is a dimer whereas the mobility of the slower dG_8 band is slightly less than dA_{28} and dC_{28} samples, suggesting a tetramer. For the oligo dG_{16} sample, the fastest band has a mobility slightly less than dA_{28} and dC_{28} oligomers, consistent with a dimeric structure.

Sedimentation equilibrium analysis was used to further characterize the state of association of the oligo dG_8 and dG_{16} samples. The curved nature of the log(OD) versus radius squared plot (Fig. 9 *B*) is diagnostic of multiple molecular masses. On the basis of the gel electrophoretic analysis suggesting dimers, tetramers, and larger species, the sedimentation data were fitted assuming a nonequilibrium mixture of dimer, tetramer, and dodecamers. The lines

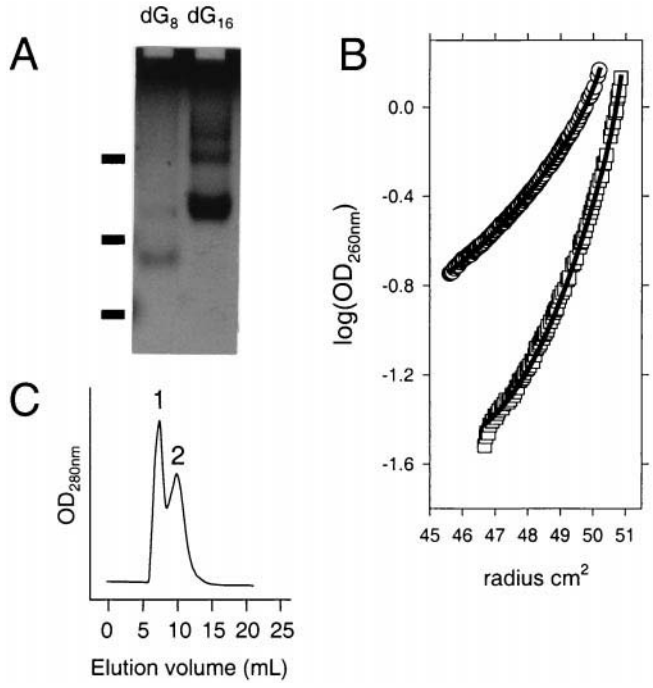

FIGURE 9 Characterization of the multimeric nature of the oligo dG_8 and dG_{16}. (*A*) Polyacrylamide gel electrophoresis of the dG_8 and dG_{16}. DNA was visualized by UV shadowing. Reference mobilities are indicated by the bars on the left of the gel, xylene green (*top*), bromophenol blue (*middle*), and orange G (*bottom*). (*B*) Sedimentation equilibrium analysis at 30,000 rpm of dG_8 (○) and dG_{16} (□). The solid lines represent theoretical fits to a dimer, tetramer, and dodecamer model. (*C*) Analysis of oligo dG_{16} by gel filtration chromatography using Sephadex G-50. Samples from peaks 1 and 2 were collected.

through the data points in Fig. 9 *B* represent best fits for oligo dG_{16} indicating 66% dimer, 28% tetramer, and 6% dodecamer and for oligo dG_8 indicating 79% dimer, 15% tetramer, and 6% dodecamer.

A difficulty with sedimentation equilibrium analysis is the problem of unequivocally assigning a model to complex data. Further characterization of the molecular heterogeneity of the oligo dG_{16} sample involved gel filtration chromatography to fractionate the sample, yielding two peaks in the elution profile (Fig. 9 *C*). The elution volumes of the oligo dG samples from these peaks remained constant for periods of at least 1 week at 4°C. Sedimentation equilibrium analysis of the sample from peak 2 indicated a single molecular mass species with a buoyant molecular mass of 4710. Given the compositional molecular mass of oligo dG_{16} (5129) we deduced that this species was a dimer (molecular mass 10258) with an apparent partial specific volume of 0.54 ml/g (Table 1). Continuous mass distribution analysis (Schuck, 2000) of the sedimentation velocity data for this sample (Fig. 10 *A*) reveals one major species of molecular mass of 10,000 (f/f_0 = 1.4; rmsd = 0.0075), consistent with the sedimentation equilibrium data.

Sedimentation equilibrium analysis of the sample from peak 1 indicates residual molecular mass heterogeneity.

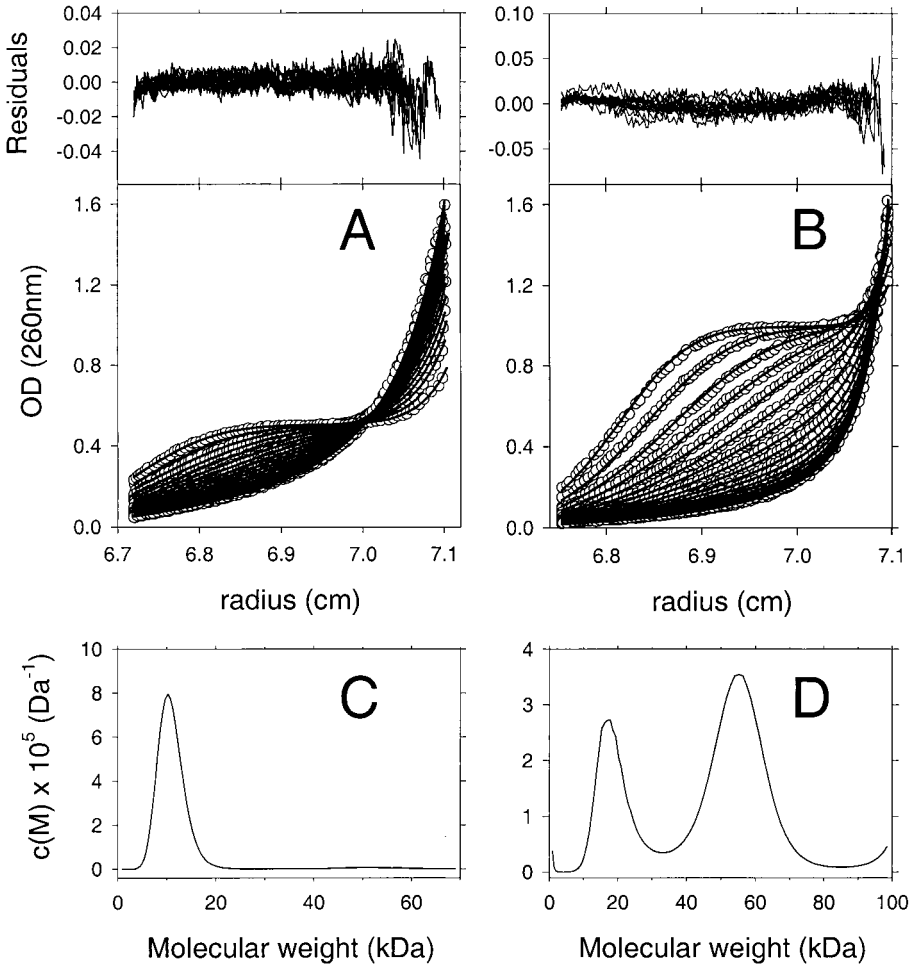

FIGURE 10 Sedimentation velocity profiles for oligo dG_{16} from gel filtration chromatography (Fig. 9 *C*). (*A* and *B*) Data for peaks 2 and 1, respectively (○). The data were fitted to continuous mass distributions yielding the profiles shown in *C* and *D*. The fits to these distributions are shown in *A* and *B* as solid lines and by the residuals.

This was further defined by continuous mass distribution analysis of the sedimentation velocity data collected during the approach to equilibrium (Fig. 10 *B*). The results, based on a partial specific volume of 0.54 ml/g, reveal a best fit with f/f_0 equal to 1.7 (rmsd = 0.013) and the presence of two predominant species of molecular masses ~17,000–20,000 and 55,000–60,000. Taken together, the data for samples 1 and 2 show that the predominant species present in the oligo dG_{16} sample are dimers (molecular mass = 10,258), tetramers (molecular mass = 20,516), and higher polymers in the range of decamers (molecular mass = 51,290) or dodecamers (molecular mass = 61,546).

DISCUSSION

Three models have been used to interpret the sedimentation velocity data for the dA, dT, and dC oligonucleotides. The first approach was to compare the experimental values for the sedimentation coefficients with theoretical values calculated for assumed helical structures. The value assigned to the radius of the atomic elements was an average based on an analysis of 13 well characterized proteins (Garcia de la Torre et al., 2000). An interesting observation from these calculations (Fig. 2) is that the computed values for the 8-mers are essentially independent of the assumed conformation, suggesting that these oligomers are isotropic. This is consistent with previous studies of short double-stranded oligonucleotides and provides the basis for estimating the degree of hydration of oligonucleotides (Bonifacio et al., 1997). The value of hydration used in the present work (0.9 g/g) underlies the values calculated for axial ratios based on a prolate ellipsoid model (Fig. 3) and the rise per nucleotide and width for an assumed cylindrical shape (Table 2). The reported variation for the degree of hydration of DNA from 0.8 to 1.0 g/g (Bonifacio et al., 1997) would lead to variations in these values. For example, in the case of oligo dT_{28}, an increase in the degree of hydration of 10% leads to changes in the axial ratio and rise per nucleotide and width for an assumed cylindrical shape of −9%, 6%, and −6%, respectively. Reciprocal changes in these values are observed for a 10% decrease in the degree of hydration. Support for the value used in the present work is provided by our results for the $dA_{16}.dT_{16}$ duplex, which gives dimensions close to that expected for B-DNA geometry. The three

models used in the interpretation of the sedimentation velocity data lead to the same conclusion that dA oligonucleotides are more rigid and extended than the corresponding dC and dT oligonucleotides. The relative compactness of the dC and dT oligonucleotides may be due to a more A-like DNA conformation, although it seems equally likely that there is greater chain flexibility compared with the corresponding dA oligonucleotides. The different solution structures of the homo-oligonucleotides need to be considered in calculations of the energetics of duplex formation (Holbrook et al., 1999). The smaller rise per nucleotide for dT oligonucleotides (0.23 nm) compared with dA oligonucleotides may underlie the inherent tendency for "A tract" curvature (Nadeau and Crothers, 1989).

Oligonucleotides containing 24 or 28 dC residues assembled into an i-motif below ~15–20°C without any significant self-association. The fourfold reduction in axial ratio (Fig. 6) is consistent with the formation of a four-stranded i-motif configuration. These data suggest that pure dC oligonucleotides can form monomeric i-motif structures without heterologous nucleotides in the loops, such as dT or dA residues. Our data show that i-motifs form at the relatively high pH of 7.4 compared with most reports of pH 7.0 and lower. The i-motif is less stable at higher pH values due to deprotonation of the cytosine base (Manzini et al., 1994). Lack of reports at higher pH values may also be due to the high proton exchange rate that prevents the detection of putative i-motif by NMR. At pH 6.0, i-motifs are more stable and more readily identified by NMR, although self-association becomes evident (results not shown). Further stability of the i-motif at pH 7.4 was achieved by extending the number of dC residues to 40. The transition temperature for dC_{40}, measured by differential scanning calorimetry was 25°C compared with the value of 20.7°C determined for oligo dC_{28} (Fig. 5 *B*). Presumably in more complex DNA sequences the stability of i-motif formation in C-rich regions in vivo may be increased by adjacent Watson-Crick base pairs.

The results in Figs. 9 and 10 show that homo-oligonucleotides composed of 8 or 16 dG residues self-associate to form mixtures of dimer, tetramer, and higher oligomer. Characterization of the thermal stability of these oligomeric species using differential scanning calorimetry and hyperchromicity experiments indicate very stable structures with melting temperatures in excess of 90°C (results not shown). Our observations are consistent with previous reports of parallel and anti-parallel quadruplex formation by mixed G-rich oligonucleotide sequences where T residues are frequently observed in the loop regions (Kang et al., 1992). The absence of any evidence of monomeric forms of oligo dG_8 or dG_{16} contrasts with the results with dA, dC, and dT oligonucleotides and suggests a strong preference for intermolecular hydrogen bonding. Hypothetical structures for the oligo dG_{16} oligomers are presented in Fig. 11. Dimeric oligo dG_{16} is best explained by either parallel or anti-parallel quadruplex formation via two hairpins (Fig. 11 *A*). Alternative

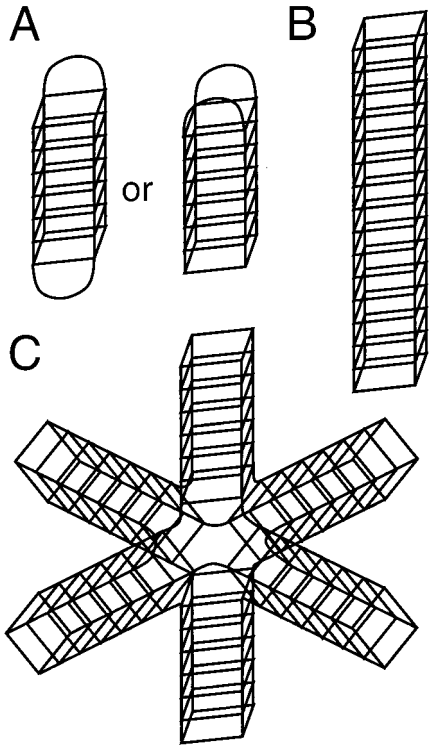

FIGURE 11 Model for oligo dG_{16} self-association. (*A*) A dimer of haipins in either a parallel or anti-parallel orientation; (*B*) A tetramer of single strands; (*C*) A dodecamer in a six-pointed star configuration.

double-stranded duplex structures seem unlikely on structural grounds and are inconsistent with the measured frictional coefficient ratio (f/f_0 = 1.4), which supports a more compact structure than the $dA_{16}.dT_{16}$ duplex (f/f_0 = 1.64). The capacity of oligo dG_8 to form a stable dimer suggests that eight residues are sufficient to form quadruplexes similar to those shown in Fig. 11 *A*. Tetrameric dG_{16} can be explained by the self-association of four linear strands of dG_{16} (Fig. 11 *B*) although the possibility that tetramers from by self-association of dG residues in the loops of dimeric quadruplexes (Fig. 11 *A*) cannot be ruled out. The higher oligomer of oligo dG_{16} has a molecular mass in the range of decamers and dodecamers. The association of 12 strands to form a dodecamer can be rationalized by the formation of the structure represented diagrammatically shown in Fig. 11 *C*. This six-pointed star geometry represents a unique variation that encompasses many of the known structural characteristics of G-quadruplex formation. These structures may be compared with the four-pointed star configuration reported for synapsable DNA duplexes formed by introducing a block of G.G mismatches into Watson-Crick double-stranded DNA helices (Fahlman and Sen, 1998). The ability of homo-oligonucleotides composed of dG or dC residues to form novel folds has potential for the identification of proteins that bind to unusual DNA

structures (Uliel et al., 2000) and in the design of oligonucleotides for pharmaceutical applications.

We are grateful to Peter Schuck, from the National Institutes of Health, Bethesda, MD, for providing computer programs and for his valuable advice during the preparation of this manuscript.

This work was funded by the National Health and Medical Research Council and the Australian Research Council. D.M.H. is the recipient of a Melbourne Research Scholarship.

REFERENCES

Ahmed, S., and E. Henderson. 1992. Formation of novel hairpin structures by telomeric C-strand oligonucleotides. *Nucleic Acids Res.* 20:507–511.

Arnott, S., Bond, P. J., Selsing, E., and P. J. C. Smith. 1976. Models of triple-stranded polynucleotides with optimised stereochemistry. *Nucleic Acids Res.* 3:2459–2470.

Bartels, C., T-H. Xia, M. Billeter, P. Güntert, and K. Wüthrich. 1995. The program XEASY for computer-supported NMR spectral analysis of biological macromolecules. *J. Biomolecular NMR.* 5:1–10.

Blackburn, E. H. 1984. The molecular structure of centromeres and telomeres. *Annu. Rev. Biochem.* 53:163–194.

Bonifacio, G. F., T. Brown, G. L. Conn, and A. N. Lane. 1997. Comparison of the electrophoretic and hydrodynamic properties of DNA and RNA oligonucleotide duplexes. *Biophys. J.* 73:1532–1538.

Cantor, C. R., M. M. Warshaw, and H. Shapiro. 1970. Oligonucleotide interactions. III. Circular dichroism studies of the conformation of deoxyoligonucleotides. *Biopolymers.* 9:1059–1077.

Cassani, G. R., and F. J. Bollum. 1969. Oligodeoxythymidylate: polydeoxyadenylate and oligodeoxyadenylate:polydeoxythymidylate interactions. *Biochemistry.* 8:3928–3936.

Catasti, P., X. Chen, R. K. Moyzis, E. M. Bradbury, and G. Gupta. 1996. Structure-function correlations of the insulin-linked polymorphic region. *J. Mol. Biol.* 264:534–545.

Chakrabarti, M. C., and F. P. Schwartz. 1999. Thermal stability of PNA/DNA and DNA/DNA duplexes by differential scanning calorimetry. *Nucleic Acids Res.* 27:4801–4806.

Chen, X., S. V. S. Mariappan, P. Catasti, R. Ratliff, R. K. Moyzis, A. Laayoun, S. S. Smith, E. M. Bradbury, and G. Gupta. 1995. Hairpins are formed by the single DNA strands of the fragile X triplet repeats: structure and biological implications. *Proc. Natl. Acad. Sci. U.S.A.* 92:5199–5203.

Durchschlag, H. 1986. Specific volumes of biological macromolecules and some other molecules of biological interest. *In* Thermodynamic Data for Biochemistry and Biotechnology. H.-J. Hinz, editor. Chap. 3. Springer-Verlag, New York. 45–115.

Fahlman, R. P., and D. Sen. 1998. Cation-regulated self-association of "synapsable" DNA duplexes. *J. Mol. Biol.* 280:237–244.

Ferrer, N., F. Azorin, A. Villasante, C. Gutierrez, and J. P. Abad. 1995. Centromeric dodeca-satellite DNA sequences form fold-back structures. *J. Mol. Biol.* 245:8–21.

Garcia de la Torre, J., M. L. Huertas, and B. Carrasco. 2000. Calculation of hydrodynamic properties of globular proteins from their atomic-level structure. *Biophys. J.* 78:719–730.

Gehring, K., J.-L. Leroy, and M. Gueron. 1993. Acid multimers of oligodeoxycytidine strands: stoichiometry, base-pair characterization, and proton exchange properties. *Nature.* 363:561–565.

Guo, Q., M. Lu, and N. R. Kallenbach. 1993. Effect of thymine tract length on the structure and stability of model telomeric sequences. *Biochemistry.* 32:3596–3603.

Guzzo-Pernell, N., J. M. Lawlor, and J. Haralambidis. 1997. Triple helical DNA. *Biomed. Pept. Proteins Nucleic Acids.* 2:107–122.

Han, X., J-L. Leroy, and M. Gueron. 1998. An intramolecular i-motif: the solution structure and base-pair opening kinetics of d(5mCCT$_3$CCT$_3$ACCT$_3$CC). *J. Mol. Biol.* 278:949–965.

Holbrook, J. A., M. W. Capp, R. M. Saecker, and M. T. Record, Jr. 1999. Enthalpy and heat capacity changes for formation of an oligomeric DNA duplex: interpretation in terms of coupled processes of formation and association of single-stranded helices. *Biochemistry.* 38:8409–8422.

Howell, R. M., K. J. Woodford, M. N. Weitzmann, and K. Usdin. 1996. The chicken β-globin gene promoter forms a novel "cinched" tetrahelical structure. *J. Biol. Chem.* 271:5208–5214.

Kang, C., X. Zhang, R. Ratliff, R. Moyzis, and A. Rich. 1992. Crystal structure of four-stranded *Oxytricha* telomeric DNA. *Nature.* 356: 126–131.

Kettani, A., R. A. Kumar, and D. J. Patel. 1995. Solution structure of a DNA quadruplex containing the fragile X syndrome triplet repeat. *J. Mol. Biol.* 254:638–656.

Langridge, R., and A. Rich. 1963. Molecular structure of helical polycytidylic acid. *Nature.* 198:725–728.

Laue, T. M., B. D. Shah, T. M. Ridgeway, and S. L. Pelletier. 1992. Analytical Ultracentrifugation in Biochemistry and Polymer Science. The Royal Society of Chemistry, Cambridge, UK. 90–125.

Laughlan, G., A. I. H. Murchie, D. G. Norman, M. H. Moore, P. C. E. Moody, D. M. J. Lilley, and B. Luisi. 1994. The high-resolution crystal structure of a parallel-stranded guanine tetraplex. *Science.* 265:520–524.

Leroy, J-L, Gehring, K., Kettani, A., and M. Gueron. 1993. Acid multimers of oligodeoxycytidine strands: stoichiometry, base-pair characterization, and proton exchange properties. *Biochemistry.* 32:6019–6031.

Leroy, J-L., M. Gueron, J.-L. Mergny, and C. Helene. 1994. Intramolecular folding of a fragment of the cytosine-rich strand of telomeric DNA into an i-motif. *Nucleic Acids Res.* 22:1600–1606.

Manzini, G., N. Yathindra, and L. E. Xodo. 1994. Evidence for intramolecularly folded i-DNA structures in biologically relevant CCC-repeat sequences. *Nucleic Acids Res.* 22:4634–4640.

Minton, A. P. 1994. Conservation of Signal: a new algorithm for the elimination of the reference concentration as an independently variable parameter in the analysis of sedimentation equilibrium. *In* Modern Analytical Ultracentrifugation: Acquisition and Interpretation of Data for Biological and Synthetic Polymer Systems. T. M. Schuster and T. M. Laue, editors. Birkhauser, Boston. 81–81.

Nadeau, J. G., and D. M. Crothers. 1989. Structural basis for DNA bending. *Proc. Natl. Acad. Sci. U.S.A.* 86:2622–2626.

Nonin, S., and J.-L. Leroy. 1996. Structure and conversion kinetics of a bi-stable DNA i-motif: broken symmetry in the [d(5mCCTCC)]4 tetramer. *J. Mol. Biol.* 261:399–414.

Olsthoorn, C. S. M., L. J. Bostelaar, J. F. M. De Rooij, J. H. Van Boom, and C. Altona. 1981. Circular dichroism study of stacking properties of oligodeoxyadenylates and polydeoxyadenylate. A three-state conformational model. *Eur. J. Biochem.* 115:309–321.

Phan, A. T., M. Gueron, and J.-L. Leroy. 2000. The solution structure and internal motions of a fragment of the cytidine-rich strand of the human telomere. *J. Mol. Biol.* 299:123–144.

Schuck, P. 2000. Size-distribution analysis of macromolecules by sedimentation velocity ultracentrifugation and Lamm equation modeling. *Biophys. J.* 78:1606–1619.

Schuck, P., MacPhee, C. E., and G. J. Howlett. 1998. Determination of sedimentation coefficients for small peptides. *Biophys. J.* 74:466–474.

Uliel, L., P. Weisman-Shomer, H. Oren-Jazan, T. Newcomb, L. A. Loeb, and M. Fry. 2000. Human Ku antigen tightly binds and stabilizes a tetrahelical form of the fragile X syndrome d(CGG)$_n$ expanded sequence. *J. Biol. Chem.* 275:33134–33141.

Venczel, E. A., and D. Sen. 1996. Synapsable DNA. *J. Mol. Biol.* 257: 219–224.

Weitzmann, M. N., K. J. Woodford, and K. Usdin. 1998. The mouse *Ms6-hm* hypervariable microsatellite forms a hairpin and two unusual tetraplexes. *J. Biol. Chem.* 273:30742–30749.

Wing, R., H. Drew, T. Takano, C. Broka, S. Tanaka, K. Hakura, and R. E. Dickerson. 1980. Crystal structure analysis of a complete turn of B-DNA. *Nature.* 287:755–758.

Zimmerman, S. B., G. H. Cohen, and D. R. Davies. 1975. X-ray fiber diffraction and model-building study of polyguanylic acid and polyinosinic acid. *J. Mol. Biol.* 92:181–192.